Turbulência

Atila P. Silva Freire
Programa de Engenharia Mecânica
COPPE/UFRJ

Anderson Ilha
Divisão de Metrologia Científica
Inmetro

Robert Breidenthal
Department of Aeronautics
University of Washington

Editores

ABCM – Associação Brasileira de Ciências e Engenharia Mecânica
COPPE/UFRJ – Instituto Alberto Luiz Coimbra de
Pós-Graduação e Pesquisa de Engenharia
IME – Instituto Militar de Engenharia

Coleção Cadernos de Turbulência
Turbulência, Volume 5, Tomo 2.

5^a Escola de Primavera em Transição e Turbulência
Instituto Militar de Engenharia, Rio de Janeiro
25 a 29 de setembro de 2006

Editores

Atila P. Silva Freire, *Programa de Engenharia Mecânica*, COPPE/UFRJ
Anderson Ilha, *Divisão de Metrologia Científica*, Inmetro
Robert Breidenthal, *Department of Aeronautics*, University of Washington

Ficha catalográfica preparada pela Seção de Processos Técnicos da
Biblioteca do Centro de Tecnologia da Universidade Federal do Rio de Janeiro

Escola de Primavera em Transição e Turbulência (5. : 2006: Rio de Janeiro, RJ)
Turbulência: Anais da V Escola de Primavera em Transição e Turbulência,
Rio de Janeiro, 25 a 29 de setembro de 2006 /editores Atila P. Silva Freire,
Anderson Ilha e Robert Breidenthal. Rio de Janeiro: ABCM, 2006.
V, 292 p.; 23 cm – Coleção Cadernos de Turbulência. Turbulência, V. 5)
Inclui bibliografias
1. Turbulência. 2. Mecânica dos fluidos. 3. Fenômenos de transporte.
I. Freire, Atila P. Silva II. II. V EPTT (5. : 2006: Rio de Janeiro, RJ).
III. Associação Brasileira de Ciências e Engenharia Mecânica. IV. Título. II.
Série
629.1332
E74T
ISBN

Documento preparado pelos Editores em LaTeX.
Impresso no Brasil pela Gráfica Graffito.

Contents

Preface

A I Escola de Primavera em Transição e Turbulência (ETT) foi uma iniciativa do Comitê de Ciências Térmicas da Associação Brasileira de Ciências Mecânicas (ABCM). Sonho antigo da comunidade de mecânica dos fluidos, ela se tornou realidade graças ao entusiasmo de alguns pesquisadores e ao apoio generoso de várias instituições.

O grande interesse no assunto, aliado à sua importância tecnológica, foram fatores que sempre conspiraram a favor de sua realização. De fato, por ser a turbulência de interesse geral para vários ramos do conhecimento, o atual formato da conferência sempre foi anseio natural da comunidade. Um forum onde métodos e praticas pudessem ser discutidos de modo livre se constituia em demanda legítima.

A Escola supriu essa demanda, adicionando, além disso, ao seu escopo, sessões técnicas de alto nível. Fruto principal da Escola, as notas dos mini-cursos dão origem a este livro. Preparadas com enorme dedicação por excelentes pesquisadores e professores em turbulência, elas certamente deverão servir de material didático para um grande número de cursos de pós-graduação em ciências e engenharias afins.

Este volume, portanto, reproduz praticamente na íntegra os textos apresentados na I ETT. No futuro, novas publicações semelhantes a esta serão editadas pela ABCM.

A.P.S.F.

Acknowledgments

Author Listing

Chapter 1 **page 1**

B. C. Khoo
Dept. of Mechanical Engineering
National University of Singapore
Kent Ridge
Singapore 119260

Y. T. Chew
Singapore-MIT Alliance (SMA)
4 Engineering Drive 3
Singapore 117576

Chapter 2 **page 115**

Dana Dabiri
Dept. of Aeronautics & Astronautics
University of Washington
Seattle, WA 98195
USA

Chapter 3 **page 205**

Robert Breidenthal
University of Washington
Seattle, WA 98195-2400
USA

Chapter 4 **page 223**

Aline Cotel
Dept. of Civil and Environmental Engineering
University of Michigan
Ann Arbor, MI 48109-2125
USA

Chapter 4

New Results on Turbulent Entrainment in Stratified Flows

4.1 Introduction

Transport across a stratified interface is an essential aspect of many geophysical processes. Consider a catastrophic volcanic eruption close to a large city, for example, Mount Rainier in Washington State next to the Seattle-Tacoma urban area. The winds are light and the ashes are approaching the city. How much time is available to evacuate the city? How high will the ashes rise? Will they reach the stratosphere? How will the weather be affected? These questions regarding the transport of ashes will be essential for the survival of a large number of people.

Imagine now another scenario: a large city in a valley where atmospheric conditions have created an unprecedented strong inversion above the city. The pollution levels are dramatically high, people are suffering from a variety of respiratory problems. The katabatic winds are not strong enough to penetrate through the inversion and dilute the polluted air above the city. A cost-effective way to destroy the interface has to be designed.

Similar problems not only exist in atmospheric environments, but also in oceanic and freshwater surroundings. It is important for large coastal cities to take into account tides, stratification and winds in the design of their sewage outfalls. For example, the newly redesigned Boston sewage outfall takes advantage of summer stratification to trap effluents below the water surface. To start solving these issues, one must begin with a profound understanding of the entrainment process and the vortex dynamics at the interface. Once one can quantify these physical processes at the interface, more accurate transport models can be developed. Other possible applications of transport across stratified interfaces can include the contribution of hydrothermal plumes on the global ocean energy budget, turbidity

currents on the ocean floor, the design of lake de-stratification systems, modeling gas leaks from storage reservoirs, weather forecasting, and global climate.

Cotel and Breidenthal (1997) proposed a theoretical model to predict the turbulent entrainment rate across a stratified interface over a wide range of parameters. A new parameter was proposed in addition to the conventional Reynolds, Richardson and Schmidt numbers (Section 4.2). This parameter called persistence is the ratio of a rotational to a translational velocity pertaining to the trajectories of vortices in the vicinity of a stratified interface. To further test the validity of persistence, laboratory experiments are performed for a tilted jet with and without precession (Section 4.4) and compared to experiments with a vertical jet impinging on a stratified interface (Cotel, 1995). Furthermore, the effect of a solid boundary is examined by investigating a sloping gravity current impinging on a stratified interface (Section 4.5). The importance of the forcing mechanism, i.e. momentum versus buoyancy, is examined by studying thermals in a stratified environment (Section 4.6). The experimental techniques are described in Section 4.3.

4.2 Entrainment theory

Entrainment is defined as engulfment of tongues of fluid (Roshko, 1976). Entrainment is different from mixing, as fluid can be entrained but not mixed at the molecular level. This might happen for lower Reynolds numbers for example. With no or weak stratification in a stagnant environment, it is assumed that the entrainment velocity is proportional to the centerline velocity or some other characteristic velocity of the flow (Morton, Taylor and Turner, 1956). For example, the entrainment of surrounding fluid into a jet is directly proportional to the centerline velocity of the jet. When stratification or compressibility effects become important, other time and length scales enter the problem, the entrainment no longer follows the hypothesis of Morton *et al.* (1956). In the presence of a stratified interface, experiments have shown that in general the entrainment rate declines with increasing stratification. It is observed that the relationship between the entrainment rate and the Richardson number obeys a power law (Turner, 1973) when the Richardson number is between one and a few hundreds. The relationship is often defined as:

$$\frac{w_e}{w_1} = cRi^{\alpha} \tag{4.1}$$

where w_e is the entrainment velocity across the interface, w_1 the characteristic velocity of the impinging turbulent flow, c and α are dimensionless constants. The Richardson number Ri (the ratio of potential energy to kinetic energy) is defined in terms of the impinging turbulence quantities:

$$Ri = \frac{g'\delta}{w_1^2} \tag{4.2}$$

with g' is the buoyancy acceleration due to the density difference $\Delta\rho$. The acceleration of gravity is g. $\Delta\rho$ is the density difference across the interface. The density

of the

$$g' = \frac{\Delta\rho}{\rho} g \tag{4.3}$$

surrounding fluid is ρ. δ is the length scale of the incident turbulence at the interface and w_1, its characteristic velocity. For $Ri < 1$, the kinetic energy of the largest eddies is greater than the potential energy investment in engulfing a tongue of fluid, so there is little or no effect of stratification on entrainment. When the Richardson number is very large, the interface becomes flat, and potential energy can no longer affect the entrainment. Therefore, the entrainment rate becomes independent of Ri (Cotel and Breidenthal, 1997). Diffusion becomes the only available entrainment mechanism.

The entrainment velocity, w_e, represents the rate at which the interface is rising due to entrainment of upper layer fluid into the turbulent flow emerging from the lower layer. The dimensionless entrainment rate is defined as the ratio of the entrainment velocity w_e to the characteristic velocity w_1. In the literature, the value of the entrainment exponent α has been found to be -1/2 (Cotel *et al.*, 1997; Price, 1979), -1 (Turner, 1968; Buch, 1980), -3/2 (Baines, 1975; Schneider, 1980) or in one case -2 (Jones and Mulhearn, 1983). Linden (1973) concluded from theoretical arguments that α should be -3/2 for a vortex ring. Kumagai (1984) measured α for a plume, finding it close to -3/2. For a jet impinging on a stratified interface (Cotel *et al.*, 1997); α was measured to be -1/2. Turner (1973) also found that the value of α seemed to depend on the Schmidt or the Prandtl number from his stirring grid experiments with heat and salt. The Schmidt number, Sc, is defined to be

$$Sc = \frac{\nu}{D_m} \tag{4.4}$$

where D_m is the molecular diffusivity and ν is the kinematic viscosity. The Prandtl number, Pr, is

$$Pr = \frac{\nu}{D_t} \tag{4.5}$$

where D_t is the thermal diffusivity. When the Richardson number is less than seven, the value of α equals -3/2. If $Ri > 7$, the value of α remains -3/2 for salt stratification, but becomes -1 for heat stratification (Turner, 1973). The Reynolds number is defined by where δ and w_1 represent the characteristic length scale and velocity scale of the flow respectively, and ν is

$$Re = \frac{w_1 \delta}{\nu} \tag{4.6}$$

the kinematic viscosity.

A model was recently proposed by Cotel and Breidenthal (1997) to extend the Morton, Taylor, and Turner's (1956) entrainment hypothesis to stratified flows. It distinguishes between flows on the basis of a new parameter, T, the vortex persistence. The model postulates the existence of a vortex (or eddy) that is responsible for the entrainment. The persistence is defined to be the number of rotations this vortex completes during the time interval it moves a distance equal

to its own diameter at the interface. It is a measure of the stationarity of the vortex. T is proportional to the ratio of the rotational, w_r, the translational speed, w_t, of the entraining eddy. The translational speed is the speed at which the eddy is moving with respect to the interface. T is independent of Ri, Re or Sc), since they all can be varied separately while T is held constant. In combination with the conventional parameters of Richardson Ri, Reynolds Re and Schmidt Sc numbers, the persistence T defines the entrainment regime (Cotel, 1995; Cotel and Breidenthal, 1997).

4.3 Experimental techniques

Laser-Induced Fluorescence: The beam of an ion-argon laser is transformed into a thin sheet via a cylindrical lens. The sheet is directed towards the tank using mirrors and is located along the centerline of the tank, providing a 2-D image of the three-dimensional flow. The entrainment rate and the location of the mixed fluid are measured directly from the images recorded on a CCD camera. The entrainment velocity w_e is measured by the rate of advance of the upper interface of the mixed layer, after subtracting the displacement due to the volume flow of the jet, thermal or gravity current entering the tank. This entrainment velocity is normalized by the flow centerline speed w_1 at the interface in order to obtain the entrainment rate. The entrainment velocity is measured shortly after the beginning of a run, while the mixed layer thickness is still small compared to the flow width (Cotel, 1995).

Particle Image Velocimetry provides non-intrusive and planar flow measurements. A thin laser sheet of green light (532 nm) is positioned in the flow seeded with Titanium Oxide particles. The laser (120 mJ New Wave Research, Inc.) is pulsed at an interval of 50 ms. Simultaneously, a frame is recorded on a CCD camera. The digitized images are analyzed with a PIV processing software (Pixelflow) from General Pixels. The software determines the velocity at points on a equally spaced grid covering the region of interest. The grid spacing used is 16 pixels. Cross correlation techniques applied to an interrogation window of 32x32 pixels are used to determine the particle displacement. The average velocity of the particles is deduced from their displacement; vorticity and streamlines are calculated from that information. The disturbances on the flow are not significant, since the particles are very small. The error in the measured velocity is estimated to be ± 0.2 cm/sec. The index of refraction needs not to be matched in these experiments as the density difference between the fluids is small, on the order of a few percents.

4.4 Turbulent jet impinging on a stratified interface

4.4.1 Background

A vertical round jet is formed when fluid issues from an axisymmetric nozzle into a quiescent environment. In the near field, the jet structure consists of a curved shear layer, which separates the potential core from the ambient fluid. As the shear layer grows, the potential core is completely consumed, typically at five diameters for a density ratio of unity. Then there is a transition zone from the initial shear layer to the asymptotic jet. Eventually, the statistical properties of the turbulence approach a far-field, asymptotic level.

The far-field jet structure may be most readily revealed by the concentration field of an inert scalar. Gibson *et al.* (1977) and Dahm & Dimotakis (1987) found that the jet consists of large regions of approximately uniform fluid with arrowhead or boomerang cross sections. Presumably these regions reflect the underlying structure. Work of Mungal & O'Neil (1989) suggests that the far-field structure jumps back and forth between two modes, an axisymmetric and a helical one.

The literature on jets is extensive and only a very brief review is given above since the focus of this particular project is on tilted and tilted/precessing jets. Zhang (1999) studied the vortical structure of an inclined jet (45° angle) within a boundary layer. Schneider *et al.* (1997) obtained LDA velocity measurements and looked at the turbulent structure associated with a precessing jet in a uniform environment.

4.4.2 Experiment set-up and procedure

A water tank, 28 cm x 28 cm x 60 cm high, is divided by a horizontal sliding splitter plate into two regions, as sketched in Figure 4.1. The experimental procedure is the following. The reservoir containing the jet solution is first filled with a saline solution mixed with fluorescein dye. The conduit between the reservoir and the tank is also filled to avoid trapping air. If air were present upon opening the valve, the stratified interface would be destroyed. A saline solution equal in density to the jet solution is then poured in the lower section of the tank. Once the lower section is filled, the horizontal splitter plate is pushed in. The upper layer is filled with a lower density saline solution, whose density varies depending on the experiments. Once the fluids have settled, i.e. turbulence from the filling process has dissipated, the splitter plate is slowly withdrawn, leaving a thin, stratified interface between the two fluids of thickness equal to 0.3cm. The valve located in the vicinity of the jet nozzle is opened to start the experiment. Different nozzles have been constructed to provide a range of different tilt angles. The nozzle is attached to a disc that can be rotated at different speeds using a standard DC motor.

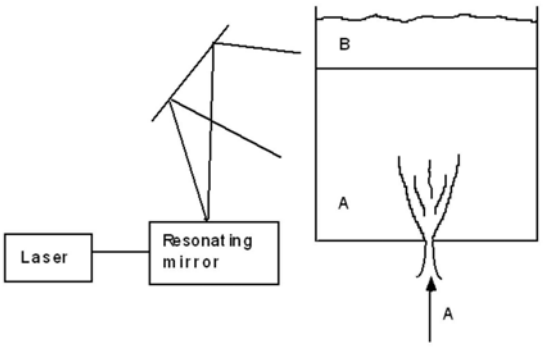

Figure 4.1: Experimental set-up for the jet experiments.

4.4.3 Results

LIF and PIV measurements are performed for a tilted jet at two different angles: 5°, 10° and compared with previous data for 15° (Cotel *et al.*, 1997). For a tilt angle of 5°, the range of Richardson was from 0.2 to 20.8 and the range of Reynolds number was from 7520 to 11700. For a tilt angle of 10°, the range of Richardson was narrowed to the region of interest, between 1.2 and 8.6. Previous work (Cotel, 1995) has shown a transition around $Ri = 10$, where the entrainment process changes from an engulfment-driven mechanism to a diffusion-dominated process. The entrainment measurements are performed soon after the impingement.

The internal waves produced at the interface during impingement do not interfere with the dynamics of the flow since no breaking of the internal waves was observed. Furthermore, the interface between the jet and surrounding fluid is sharp, diffusion does not play a significant role in the entrainment process for the range of Ri investigated.

Tilt only - No precession

The entrainment rate was measured for a jet at different tilt angles. The Richardson number is defined on the jet quantities and the initial density difference across the interface as stated above. Figure 4.2 shows the measured entrainment rates (and error bars) as a function of Ri for different jet tilt angles. The error in the entrainment law fit ranges from 0.1% (15° case) to 24% (10° case). For angles up to 10°, the entrainment rate follows the same power law, $Ri^{-1/2}$ whereas for the 15° case, the entrainment rate is now proportional to $Ri^{-3/2}$. There is no significant difference in the data for the 5° and 10° cases. There appears to be a significant change in the jet dynamics between the angles of 10° and 15°. One proposed explanation is that the half-angle of expansion, which lies between 12° and 15° for a vertical turbulent jet (Dahm and Dimotakis, 1987), is important in determining this particular transition. Laser-Induced Fluorescence is used to

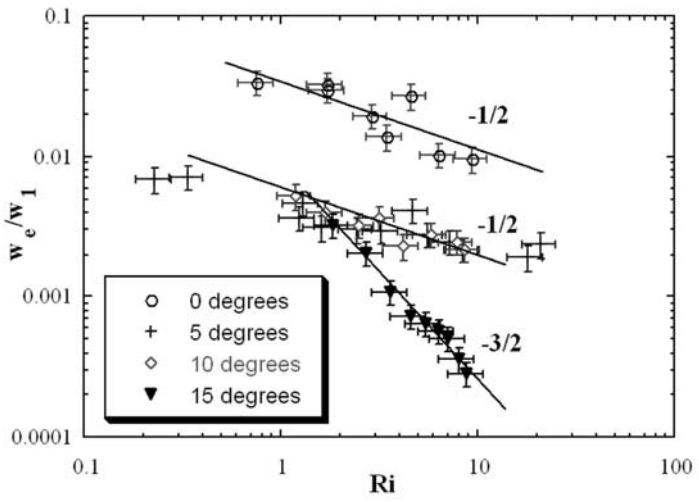

Figure 4.2: Entrainment rate versus Richardson number for different tilt angles.

visualize the internal structure of the jet at the time of impingement and to reveal any difference in baroclinic vorticity near the interface (Figure 4.3). It was demonstrated previously (Cotel *et al.*, 1997) that baroclinic vortices are responsible for the entrainment in a vertical jet impinging on a stratified interface. It seems reasonable to assume that a similar process would occur in the case of a tilted jet, in particular for small angles of tilt. The baroclinic vorticity generated by the impingement process can be clearly seen in Figure 4.3. Each photograph is taken at approximately 30 s after the valve is opened and the jet has exited the nozzle located at the bottom of the tank. The bright fluid represents a mixture of upper layer and jet fluids. The tank walls do not affect the entrainment measurements as they are taken in the first few seconds after impingement to ensure no wall or internal wave effects are present.

A vertical jet impinging on a stratified interface exhibits the following structure: on each side of the dome, a strong baroclinic vortex is formed, and that vortex is responsible for entraining and mixing surrounding fluid (Cotel, 1995). For a tilt angle of 15°, this vortical structure is not fully formed, only one baroclinic vortex completely rolls up and is strong enough to entrain fluid, while the opposite side shows much weaker baroclinic vorticity. Figure 4.4(a) shows the vorticity contours for $Ri = 8.7$ and for a tilt angle of 10° before impingement. The jet vortices are clearly shown in red and blue representing the two signs of vorticity within the jet structure. In Figure 4.4(b), which represents the after-impingement situation, there is a baroclinic vortex on the left side located just above the jet vortex, rotating in opposite direction to the jet vortex. However on the right side of the image, there is no distinct baroclinic vortex above the jet vortex. Even at that

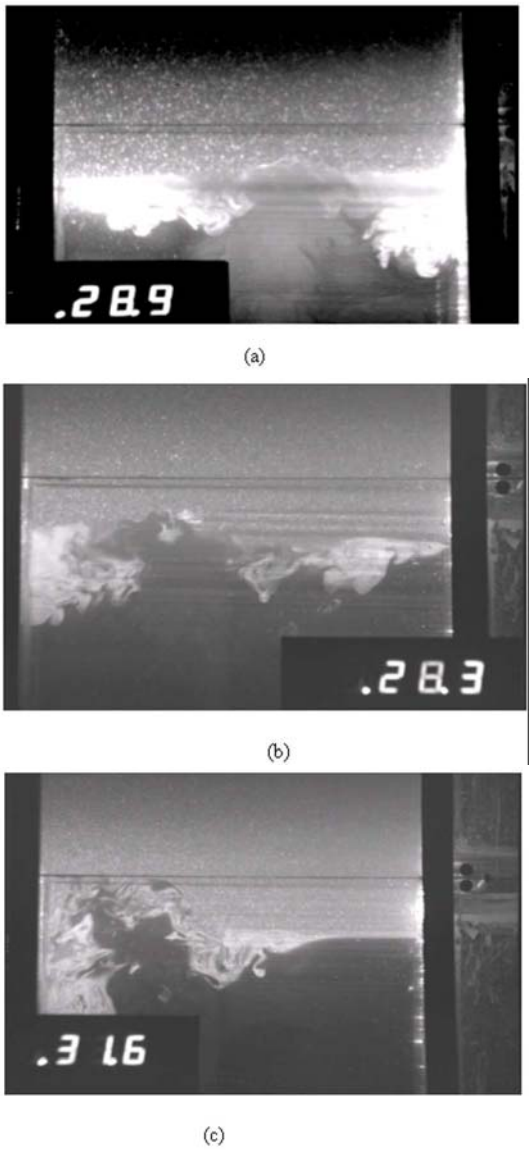

Figure 4.3: LIF photographs of tilted jet at various angles for Ri=2.5. The numbers in the images represent the time elapsed after the valve to the jet reservoir has been opened. (a)5° (b)10° (c)15°

angle, the baroclinic vorticity starts changing its dynamics and is not able to roll-up completely around the impingement dome. Figure 4.4(b) is an average of 5 image pairs, representing an average over 0.1 s given our PIV data acquisition conditions.

Furthermore, the circulation of baroclinic vorticity around the impingement dome is quantified. From PIV data averaged over 2 seconds, the area of the vortex (or vortices) and the corresponding average vorticity are determined in order to calculate circulation. Circulation, defined as the surface integral of vorticity, provides a measure of the strength of a vortex. Figure 4.5 shows a decrease of in the circulation of baroclinic vorticity as a function of tilt angle for a given Richardson number, in this case, $Ri = 8.7$. The error bars are on the order of 20% as there is some error in precisely characterizing the edge of a vortex.

As the tilt angle increases, less and less baroclinic vorticity is able to fully roll-up in the area surrounding the impingement dome. The lack of baroclinic vorticity roll-up and the decrease in the strength of the baroclinic vorticity are reflected into the decreased capacity of the jet to entrain surrounding fluid. This change of the vortical structure of the jet translates into a different entrainment regime. Both the power law exponent and the magnitude of the entrainment rate change with tilt angle. The entrainment rate of a tilted jet is at least one order of magnitude lower than that of a vertical jet.

Effect of precession

A DC motor is installed in order to provide means to rotate the jet nozzle at various angular velocities. The goal of this set of experiments is to determine the transition between entrainment regimes by only changing the vortex persistence parameter, i.e. the precessing speed.

Figure 4.6 compares the entrainment rate as a function of Richardson numbers for different values of the vortex persistence parameter. The precessing speed is varied to determine the transition from persistent to non-persistent for the 10° case. With no precession, a 10° tilted jet follows a $Ri^{-1/2}$ power law. For low values of the precessing speed, no clear pattern is observed, a significant amount of scatter is present. The entrainment is in-between persistent and non-persistent regimes. However, for a persistence parameter equal to 1/2, we found that the entrainment rate is consistently in the non-persistent regime, proportional to $Ri^{-3/2}$. It is possible to physically force a persistent regime into a non-persistent regime by imposing a large enough precessing speed. Precession is a valuable tool when a low entrainment rate is desirable in a particular situation; by manipulating the persistence parameter, a reduction on the order of two orders of magnitude in entrainment rate can be achieved.

4.4.4 Discussion

There is a direct relationship between entrainment rate for a tilted jet impinging on a stratified interface and the vortical structure surrounding the impingement

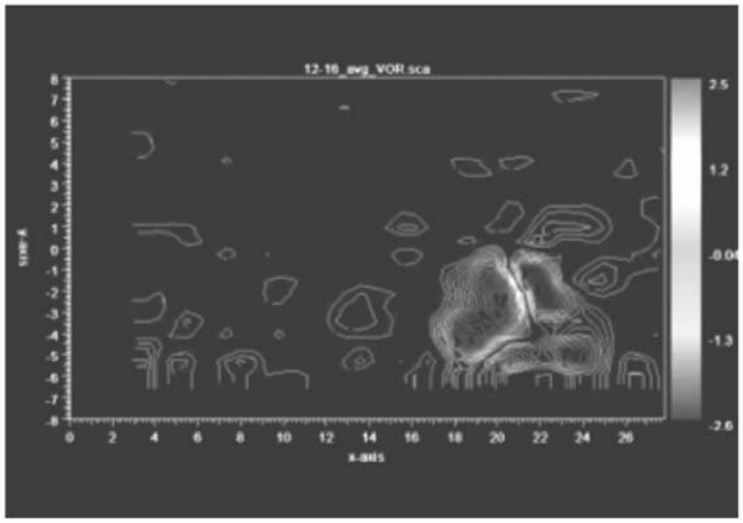

(a)

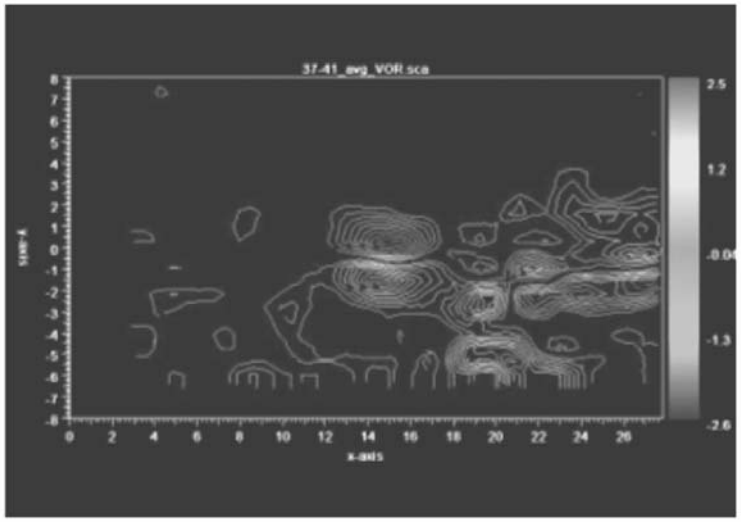

(b)

Figure 4.4: Vorticity contours (in 1/sec) from PIV data for a 10° tilted jet at Ri=8.7. The x and y axes represent the horizontal and vertical axes of the apparatus (in cm). (a)Before impingement (b) After impingement, note the formation of baroclinic vortices, counter-rotating to the jet vortices only on one side.

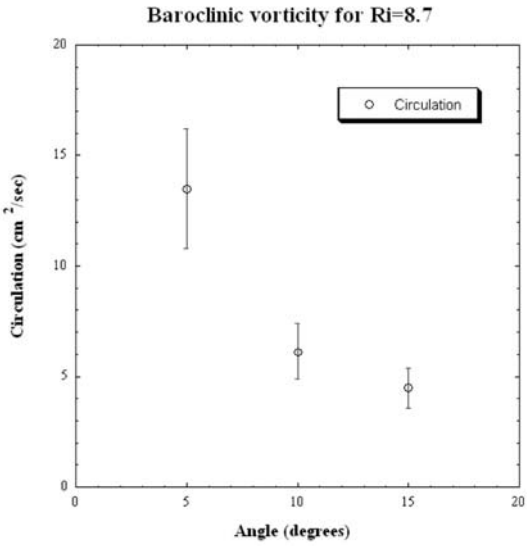

Figure 4.5: Circulation (in cm^2/sec) of baroclinic vorticity as a function of tilt angle of the jet (in degrees) for Ri=8.7.

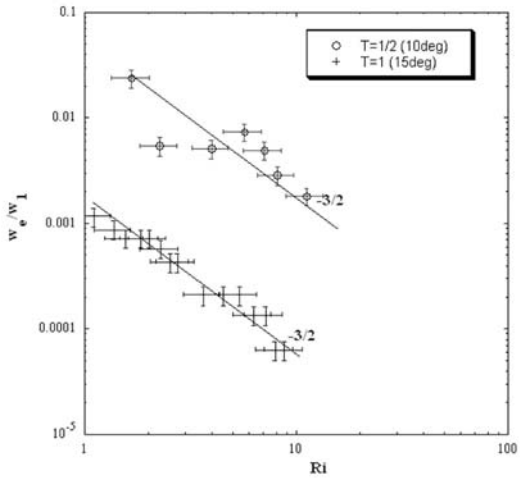

Figure 4.6: Effect of the persistence parameter on entrainment rate for a tilt angle of 10°, compared to 15° tilt.

dome. When the baroclinic vortices are stationary, the entrainment rate follows an entrainment law (proportional to $Ri^{-1/2}$) characteristic of a persistent regime, as defined by Cotel and Breidenthal (1997). The transition between persistent and non-persistent regimes occurs at an angle between 10° and 15°, which is equivalent to the half-angle of the jet. When the tilt angle is greater than the critical half-angle of the jet, the entrainment rate always exhibits a non-persistent behavior. In other words, the baroclinic vortices created at impingement are either weak or non-existent. However, when the tilt angle is smaller than the half-angle of expansion, most of the baroclinic vortices around the impingement dome complete a full rotation and greatly contribute to the entrainment. The combination of PIV and LIF measurements reveals the correlation between the presence (Figures 4.3 and 4.4) and strength of baroclinic vorticity (Figure 4.5), jet angle and entrainment rate.

At low tilt angles, it is possible to reduce the entrainment rate by imposing a large enough precessing speed. A naturally persistent regime is then forced into a non-persistent entrainment regime, therefore providing a much lower entrainment for the same values of Richardson number.

4.5 Sloping gravity currents impinging on a stratified interface

4.5.1 Background on gravity currents

Benjamin (1968) did some of the early work on gravity currents. His theoretical approach based on inviscid fluid theory provided solutions for depth and velocity of a gravity current. Previous experiments were performed in a homogeneous environment along the bottom of a tank. Measurements included growth rate, hydrodynamic instabilities, structure, such as Simpson (1982), Hallworth *et al.* (1996) Simpson (1982) described the gravity current as a succession of clefts and lobes, due to gravitational instability of the less dense fluid overrun by the nose of the current. Kelvin-Helmholtz instabilities are present in the region of the current behind the head, which is a region of intense mixing. Hot wire measurements were taken to quantify the fluxes in and out of the head of a gravity current (Winant and Bratkovich, 1977). They found that the mass flux of heavy fluid into the head is 0.15 times the flux of the current itself.

Laser-Doppler Anemometry (LDA) measurements were performed recently to map out the velocity profile and Reynolds stresses on the bottom surface (Kneller *et al.*, 1999). It was found that the dominant length scale was of the order of the thickness of the dense underflow. Fleischmann and McGrattan (1999) studied the same type of flow in the context of fire backdrafts, which behave as gravity currents. Entrainment measurements have been performed for 2-D and axisymmetric currents along a flat surface in a uniform environment, i.e. no horizontal stratification. The entrainment was found to be independent of g' and therefore of the Richardson number. The entrainment coefficient was different between 2-D

and 3-D currents, and varies with the surface of propagation, a smooth surface yielded a different entrainment constant than a rough surface (Hallworth *et al.*, 1996). The entrainment in the head of gravity current was found to only depend on the initial volume of the current and the distance from the release point.

This represents a sample of the literature on horizontal gravity currents and intrusions. The literature on this subject is extensive, however, the present experiments use a slightly different configuration, i.e. the propagation of a gravity current along an inclined slope. For gravity currents down a slope in a homogeneous environment, i.e. no density stratification, Turner (1973) found that

$$E = Ri_0 \tan\theta \tag{4.7}$$

where E is the entrainment, Ri_0 the overall Richardson number and θ the slope angle. The dynamics of a gravity current flowing downslope is changed dramatically (Hopfinger and Tochon-Danguy, 1977). The entrainment into the head increases with increasing slope (Britter and Linden, 1980). Whitehead and Chapman (1986), and Mitsudera and Baines (1992) studied the behavior of a gravity current on a sloping bottom in a linearly stratified environment. Detrained layers at different levels above the tank bottom were observed as well as shelf waves in one of the experiments. Monaghan *et al.* (1999) studied the case of gravity currents descending a ramp in a two-layer stratified tank. Different ramp angles of 20, 45 and 90 degrees were set-up. A numerical model was compared to the experiments to explain the behavior of large amplitude waves.

Hacker *et al.* (1996) performed experiments of finite volume gravity currents on a horizontal surface. They found that substantial mixing occurs in the early stages of the propagation of the current. The location of the gate separating the gravity current fluid from the ambient (uniform) environment was varied, producing different aspect ratios of total water depth to the length of the lock holding the gravity current fluid. They investigated the effect of this aspect ratio on the evolution of the flow and concluded that it has an effect on the structure of the head, but other factors such as changes in Reynolds number and the disturbance caused by the withdrawal of the gate may have also played a role. Similarly, Huq (1996) investigated experimentally the role of the initial aspect ratio (height/radius) on the dilution and entrainment rates of instantaneous releases of a dense, finite volume gravity current into a larger, sector-shaped volume of less dense fluid. The effect of increasing the aspect ratio is to increase the dilution.

The case of gravity currents in a two-layer stratified environment has been studied by others. Lowe *et al.* (2002) performed laboratory experiments in which an intrusive gravity current was observed using shadowgraph and particle tracking methods. The intrusion was generated in a two-layer fluid with a sharp interface, with the gravity current propagating along the interface. Their purpose was to determine the structure of the velocity field inside the intrusion and they concluded that the structure of the flow inside the intrusion can be divided into three regions: the head region in which the fluid velocity is nearly uniform with speed equal to the front speed, a dissipative wake region and behind that a tail region in which there is very little mixing. Monaghan *et al.* (1999) was interested on the creation

of internal waves along the stratified interface. They used different ramp angles of 20°, 45° and 90°. The results of a numerical model, using the Lagrangian particle method, were compared to the experiments to explain the behavior of large amplitude waves. Sutherland *et al.* (2004) and Flynn and Sutherland (2004) used a two-layer stratified environment for their studies. In both cases, the gravity current was propagating along the interface. Sutherland et al. (2004) compared the prediction from an analytical solution for the speed and the vertical extent of the gravity current head with experimental results. They found an excellent agreement when the density of the gravity current is the average of the upper and lower-layer densities. Flynn and Sutherland (2004) studied the vertical flux of horizontal momentum due to the generation of internal waves along the interface and related it to properties of the fluid intrusion.

4.5.2 Gravity current experiment set-up and procedure

The experiments are carried out in a 5 m long horizontal flume. The flume, made of Plexiglas, is 30 cm wide by 50 cm deep (Figure 4.7). The sloping bottom where the current is propagating is made of a thin Plexiglas sheet caulked to the sides of the flume and the slope is set at α=6°. The x-axis is considered to be along the sloping bottom, with x=0 being at the origin that is represented by the location of the gate. The location of the stratified interface is at x=1.0 m and the end of the slope (where it becomes horizontal) is at x=2.0 m. The height of the ramp at the origin (where x=0), from the bottom of the flume is 21 cm.

Saline solutions are used to achieve the density differences necessary to reach a given range of Richardson numbers. The saline solutions are prepared with the following procedure: A 55 gal tank is completely filled with fresh water and a fine sieve is placed on top of the tank, so that it is partially under the water surface. The salt is poured on the sieve and left to dissolve. As the salt dissolves the water on the surface of the tank becomes heavier and a circular motion starts in the tank, with the fresher water at the bottom replacing the heavier at the surface of the tank. With this procedure, the density of the fluid is uniform throughout the tank. The saline solution is used for the experiments in 24 to 36 hours after the salt has dissolved, to ensure that all impurities are settled at the bottom of the tank. A portion of this dense fluid is diluted with the appropriate quantity of fresh water in two different tanks, to achieve the required density of the two different dense fluids that are necessary for an experiment (gravity current fluid and bottom layer fluid). Then depending on the experiment to be performed, different chemicals are added to these two fluids. The range of density of the gravity current fluid is between 1,012 to 1,100 kg/m^3, while the range density of the bottom layer is between 1,008 to 1,022 kg/m^3. Fresh water is used for the top layer. Initially the flume is filled with the fresh layer to a height of 35 cm. The lower denser layer is set in place using a diffuser, connected to a tank of heavy, salty water.

The diffuser is made of a thin Plexiglas plate glued to a short PVC pipe into which the salty water is supplied very slowly with a pump (around 5x10^{-5} m^3/sec). This procedure prevents mixing between the two layers and creates a thin stable

stratified interface with a thickness of approximately 0.5 cm. In order to have a constant depth in all experiments, an overflow weir is placed at the downstream end of the flume (Figure 4.7). The total height of fluid in the flume is 46 cm before the release of the gravity current fluid. The reservoir is filled with the dense gravity current fluid by a pump and a lock release mechanism is used to generate two-dimensional gravity currents in the laboratory.

During the filling process of the flume and the gravity current reservoir, a gate is locked in place to separate the gravity current fluid in the reservoir from the flume containing the stratified environment; therefore no initial mixing takes place between the gravity current and the stratified environment. Once the reservoir is full with the gravity current fluid, the gate is lifted to initiate an experiment. To quantify the mixing and entrainment processes at the region of impingement,

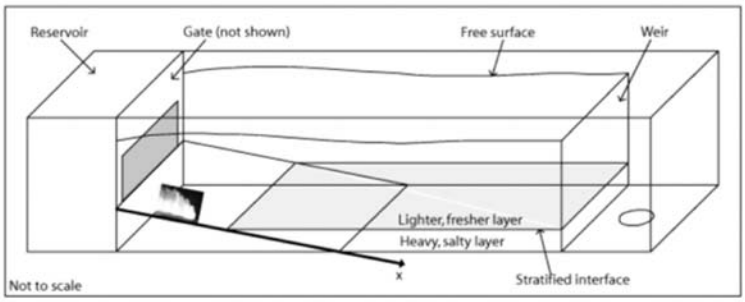

Figure 4.7: Schematic of the experimental apparatus for the gravity current experiments.

Planar Laser-Induced Fluorescence (PLIF) experiments are performed. Disodium fluorescein, whose fluorescence is pH sensitive, is used in these experiments. It is added to the gravity current fluid with a concentration of $7.5\text{x}10^{-4}$ grams per liter of dense fluid, together with sulfuric acid (H_2SO_4) with a concentration of 4 mlit per liter of dense fluid. The pH of the solution is lowered to around 3. When sodium hydroxide (NaOH) is added to the bottom layer (1 mlit per liter of fluid), mixing between the different fluids is visualized with an ion-argon laser. No chemicals are added to the top layer fluid and the pH is at 7. The beam of the laser is transformed into a thin sheet through a pair of cylindrical lens with focal length f=-12.7 mm.

4.5.3 Parameters

It is necessary to define the parameters that govern the propagation of a gravity current on a slope at an angle α to the horizontal (Figure 4.8). The Reynolds number is in the range of 4,000 to 15,000 and is defined as:

$$Re = \frac{U_f d}{\nu} \tag{4.8}$$

where U_f and d are the characteristic velocity and height of the head of the gravity current before the impingement and ν is the kinematic viscosity of water.

Accordingly the Richardson number is defined by the characteristics of the head before the impingement:

$$Ri = g\frac{\Delta\rho}{\rho}\frac{d}{U_f^2}\cos\alpha \tag{4.9}$$

where g is the acceleration of gravity and $\Delta\rho$ is a density difference. There are three different ways for the Richardson number to be defined, depending on the choice of $\Delta\rho$ (Samothrakis and Cotel, 2006). When $\Delta\rho$ is defined by the density difference between the current and top layer fluids, $Ri_{(C-T)}$ determines the velocity and height of the head of the gravity current before the impingement. The balance between the initialbuoyancy and the characteristics (velocity and height of the head) of the gravity current is represented by $Ri_{(C-T)}$. The second one, $Ri_{(B-C)}$, is defined by the density difference between the current and bottom layer fluids. After the impingement, the gravity current encounters the bottom layer fluid and their density difference is taken into account through $Ri_{(B-C)}$. This definition of Ri number governs the rate by which bottom-layer fluid is entrained into the gravity current. Finally the third one, $Ri_{(B-T)}$, is defined by the density difference between the bottom and top layer fluids. This definition of Ri number represents the relative strength of the interface with respect to the energy of the gravity current acquired before the impingement and the easiness by which the gravity current penetrates the interface.

The range of the $Ri_{(B-C)}$ and $Ri_{(B-T)}$ numbers is highly affected by the velocity of the gravity current (which is squared in the definition). When a large density difference between the gravity current fluid and the ambient layers is used, the velocity is high, producing small Ri numbers. With a small density difference between the gravity current fluid and the ambient layers, the velocity is small and the resulting Ri number is high.

As our interest is on penetrating gravity currents, there is a limit in the density difference that can be used and therefore the upper limit of the range of Ri is dictated by the physical constraints of the experimental set-up.

4.5.4 Results

The following procedure was used: before a series of experiments, a ruler is placed at the location of the laser sheet and the magnification is calculated (in terms of pixels/cm). The number of pixels that correspond to a certain dimension on the picture (like the height d of the head, or the location x of the head) is obtained through image processing. Based on the size of the images (776x484 pixels), the uncertainty is estimated to be ± 0.60 pixels or (with a typical magnification of 15px/cm) $\pm 0.4mm$.

Constant flux: The typical lobes and clefts structures (Simpson, 1997) are observed along the upper surface of the gravity current head. As a result fluctuations are seen in this area. When the flow is visualized with dye or shadowgraph, it is

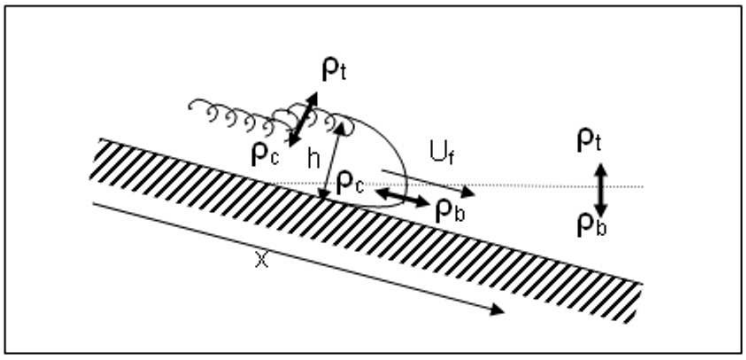

Figure 4.8: Sketch of a gravity current on a slope, with an initial head followed by a steady layer flow. Various variables are defined.

more difficult to define the height and location of the head. But for the measurements based on the PLIF images, where a slice of the flow is visualized, the height/location of the head is easily determined through image processing. The velocity of the gravity current, U_f and the height d of its head were measured for all the experiments, before the impingement, when the nose of the gravity current head is just touching the interface at $x = 1.0$m. The velocity of the gravity current, U_f , compares very well with previous studies (Britter and Linden, 1980). This shows that the gravity current is well developed when it hits the interface and the effect of friction is negligible in our experiments.

Figure 4.9 shows a photographic sequence of the gravity current, visualized by the PLIF technique. It can be seen from the images that there are two mechanisms responsible for mixing. The first one is the over-riding and engulfment of ambient fluid beneath the nose of the head. There is no mixing at the front of the current. Similarly Johari (1992) for the case of a thermal observed that the volume of entrained fluid by the small-scale eddies on the front of the thermal is small compared to the entrainment by the large-scale eddies in the perimeter of the thermal. Furthermore, these large eddies are responsible for entraining surrounding fluid and bringing it to the center of the thermal where it is ultimately mixed. This is similar to the process of overriding and engulfment in the case of the gravity current. The second mixing mechanism is due to the Kelvin-Helmholtz instabilities along the upper surface of the head (Britter & Simpson, 1978). This confirms that the Kelvin-Helmholtz vortices, formed on the upper surface of the head, represent the dominant mixing mechanism. Similar observations have been reported in other turbulent flows by Brown and Roshko (1974), Dahm and Dimotakis (1987) and Papantoniou and List (1989). In Figures 4.9(c) and 4.9(d) we can see more details of the flow, e.g. two large structures following one another. Hallworth *et al.* (1996) measured the entrainment for a two-dimensional,

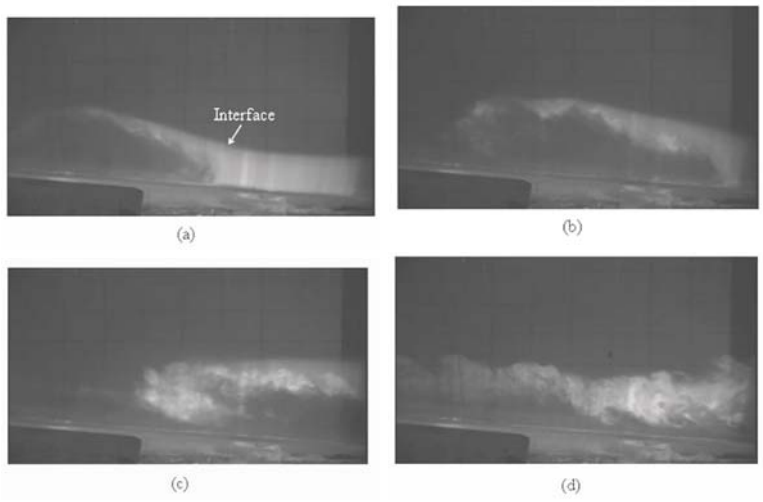

Figure 4.9: Sequence of PLIF images for a constant flux gravity current (Re=10,500 and Ri(B-C)=1.8).

constant-volume gravity current, as the ratio of the volume of ambient fluid to the initial volume of the gravity current in the head. For the case of a constant-flux gravity current, Britter and Linden (1980) defined the entrainment as the rate of change of the head height. The rate of growth of the head $dh = dx$ was measured using Planar Laser Induced Fluorescence, with h being the height of the head and x the downstream distance along the slope. This ratio was measured at two different locations to ensure that the effect of the interface on the entrainment of the gravity current is considered. The first one is at a distance 10 to 30 cm after the interface and the second one at a distance 60 to 80 cm after the. The rate of growth of the head at the two locations is found to be proportional to $Ri_{(B-C)}^{-1\pm.1}$ (Figure 4.10). As the gravity current is propagating through the bottom layer, the density difference of the two fluids controls the entrainment rate between them.

Also, both the velocity and height of the gravity current before the impingement affect the entrainment rate. These parameters are implicitly included in $Ri_{(B-C)}$. The relevant Ri is based on the difference between the current and the bottom layer. The entrainment we are interested in quantifying is the entrainment of lower or bottom layer fluid into the gravity current. Implicitly, the density of the top layer is important as it defines the gravity current velocity and size before impingement. Therefore, the relevant Ri combines the density of the gravity current, its size and velocity; and the density of the bottom layer. Finally, it should be noted that the range of variation of the Ri number is close to a decade. The range is limited due to constraints linked to the experimental apparatus.

Finite volume: A photographic sequence of the gravity current taken from the

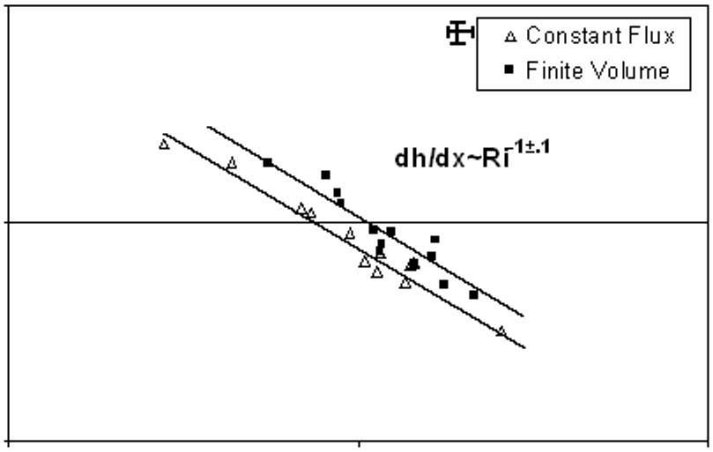

Figure 4.10: Comparison of head growth rate for constant flux and finite volume gravity currents.

Planar Laser Induced Fluorescence experiments is shown in Figure 4.11. In Figure 4.11(a) the location of the interface is marked and the gravity current can be seen entering the image from the left. The color of the gravity current fluid is grey, as it has not yet mixed with the bottom layer fluid. When the mixing between these two fluids occurs (Figures 4.11(b), 4.11(c) and 4.11(d)), the dye in the gravity current fluid fluoresces abruptly. In Figure 4.11(b) the two mechanisms responsible for mixing are observed for the case of a finite volume gravity current. The first mixing mechanism is the overriding of ambient fluid by the gravity current head (marked as location 1 in Figure 4.11(b). The second one is the Kelvin-Helmholtz instabilities (Britter and Simpson, 1978) that appear on the upper surface of the head (marked as location 2 in Figure 4.11(b)). The Kelvin-Helmholtz vortices represent the dominant entrainment and mixing mechanism, responsible for the bulk of the mixing.

Figure 4.12 provides a more detailed view of the mixing occurring during impingement. The top image in Figure 4.12(b) is a magnified picture of the area in the black rectangle of Figure 4.12(a), where an eddy is being formed. The rest of the images in column (b) are 0.2 sec apart and provide a magnified picture of the same eddy as it propagates downstream. We can clearly see in the top image of column (b), the process of bottom layer fluid being entrained in the gravity current head. Then the fluid is brought to the core of the vortex and finally, in the last image of the sequence of Figure 4.12(b), being mixed. Each pixel of the PLIF images (Figure 4.11) has a corresponding light intensity with a range from 0 (black) to 255 (white). With image processing, the range of light intensity that corresponds to the mixed fluid can be determined. In each image, the number of pixels that lie in this range of mixed fluid is measured and with the given magnification (in terms

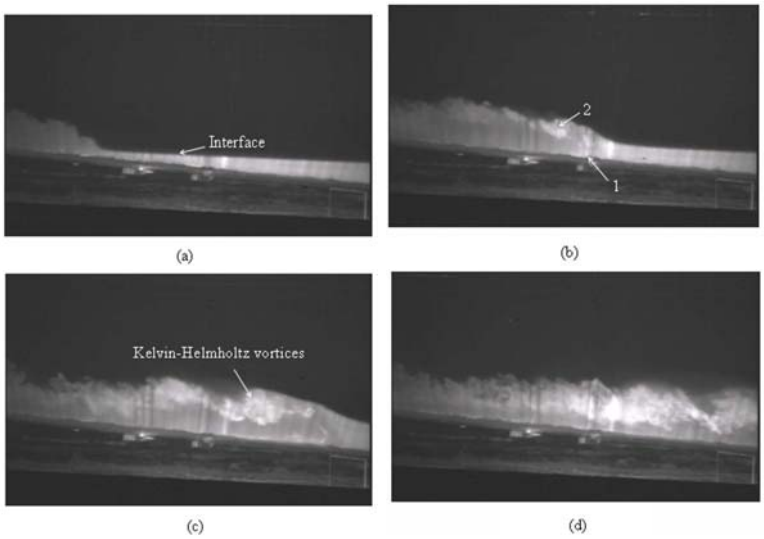

Figure 4.11: Sequence of PLIF images, 2 seconds apart for a finite volume gravity current (Re=10,000 and $Ri_{(B-C)}$=*0.7)*

of pixels/cm), the area of mixed fluid in each picture is evaluated and the volume per unit width of mixed fluid, V_{mix}, in each picture is then deduced. The ratio of the volume of mixed fluid, V_{mix}, to the initial volume of the gravity current, Vo, is plotted versus the Richardson number in Figure 4.13 at four different locations of the tip of the gravity current head. These four locations are 105, 115, 125 and 135 cm downstream of the origin (defined as the beginning of the ramp) or 5, 15, 25 and 35 cm downstream of the location of impingement. For all four locations, the ratio of mixed fluid to the initial volume of gravity current fluid, $V_{mix} = Vo$ is found to be proportional to $Ri_{(B-C)}^{-1\pm.15}$ (Figure 4.13). The difference in the measured values is due to the fact that as the gravity current fluid is propagating deeper into the bottom layer, the volume of mixed fluid is increasing (i.e. more bottom fluid is entrained into the gravity current head). Error estimates are provided in the upper right corner of the graph. The entrainment measurements were taken at a distance 10 to 30 cm after the interface. In Figure 4.10, the rate of growth of the head of a finite volume gravity current is plotted versus Richardson number and is found to be proportional to $Ri_{(B-C)}^{-1\pm.1}$. Error estimates are provided in the upper right corner of the graph.

Both the ratio of mixed fluid to the initial volume of gravity current fluid $V_{mix} = Vo$ (i.e. the mixing rate) and the rate of growth of the head $dh = dx$ (i.e. the entrainment rate), are found to be proportional to $Ri_{(B-C)}^{-1}$. The Ri number governing the entrainment and mixing rate is based on the difference between the current and the bottom layer, since we are interested in quantifying

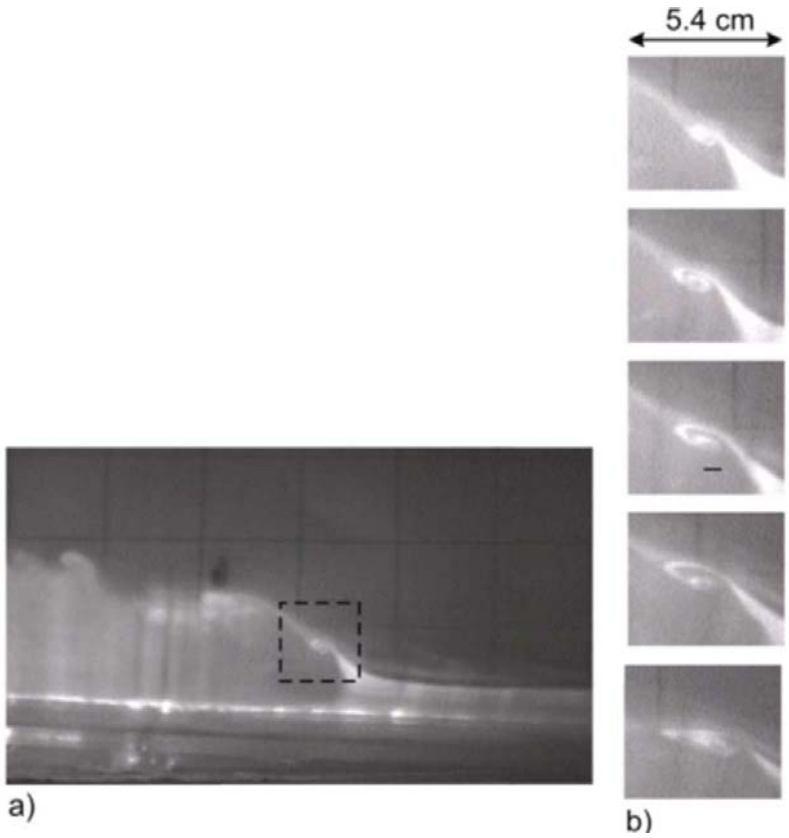

Figure 4.12: Details of the mixing process from PLIF images. The images in column b) are 0.2 seconds part (Re=6,000 and $Ri_{(B-C)}$=0.4)

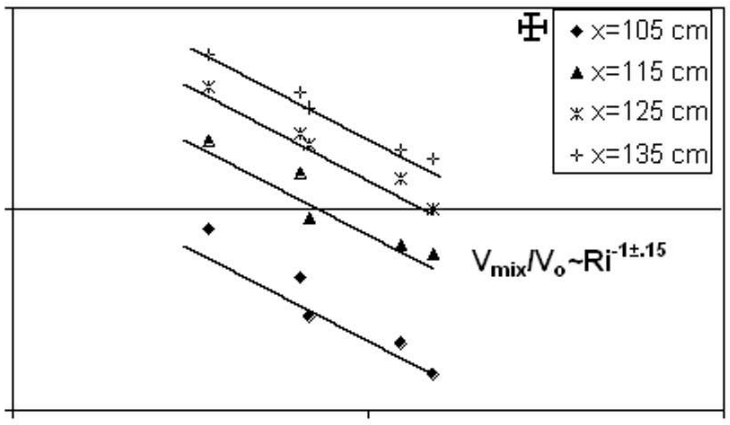

Figure 4.13: Ratio of mixed fluid to initial volume of gravity current fluid versus Richardson number at 4 different locations. The location of impingement is at x=100cm.

the entrainment/mixing of lower or bottom layer fluid into the gravity current.

4.5.5 Discussion

For both cases of a constant flux gravity current and a finite volume gravity current impinging on a stratified interface, we observed that the Kelvin-Helmholtz vortices, formed on the upper surface of the head of the gravity current, represent the main mixing mechanism. In terms of the mixing and entrainment rates, we found that both are proportional to $Ri^{-1}_{(B-C)}$ which corresponds to a shear-dominated regime (Figures 4.10 and 4.13). Finally, as the Reynolds number for all the experiments was above the mixing transition, the entrainment and mixing are proportional to each other (Breidenthal and Baker, 1985; Cotel et al, 1997). In Figure 4.13 a comparison of the rate of growth of the head between the cases of constant flux and finite volume gravity currents, is presented. Details of the measurements for the constant flux case can be in found in Samothrakis and Cotel (2006) and Samothrakis (2005). The measured values for the case of the finite volume gravity current are slightly higher, but the difference is close to our estimated error. Part of the difference can be attributed to the fact that in general the velocity of a finite volume gravity current is smaller compared to a constant flux one. Therefore, as it penetrates the interface with a smaller velocity and encounters the denser bottom layer fluid, it spreads more (slightly higher values of $dh = dx$) than a constant flux gravity current. The initial volume used in our experiments is within the range of volumes used by previous researchers for finite volume gravity current experiments (Huppert & Simpson, 1980; Beghin *et al.*, 1981; Hallworth *et al.*, 1996; Monaghan,

1996; Monaghan *et al.*, 1999; Hacker, *et al.*, 1996; Huq, 1996; Lowe *et al.*, 2002; Maxworthy *et al.*, 2002; Sutherland *et al.*, 2004). Therefore, the volume used in our experiments (14,000 cm^3) represents a finite volume gravity current based on previous work.

4.6 Thermal/plume impinging on a stratified interface

4.6.1 Background on thermals

The term "thermal" is used to denote a parcel of isolated buoyant fluid suddenly released from rest, which subsequently moves under the action of buoyancy forces alone. An isolated thermal represents a purely convective flow in the atmosphere, with absolutely no momentum, circulation, or kinetic energy initially present in the flow (Woodward, 1959). From the motion of cumulus clouds, it appears that convection, which is produced by buoyancy forces, consists largely of more or less isolated masses of buoyant air rising into and mixing with their surroundings (Scorer, 1957). Characterized by its total buoyancy force, a thermal acquires circulation, kinetic energy, and momentum as it accelerates in the near field. The circulation is generated entirely by buoyancy after the thermal is released. In laboratory experiments, buoyancy force is conveniently induced by salinity differences. Scorer (1957), Woodward (1959), and Turner (1963) performed tank experiments involving heavy brine parcels sinking through a uniform environment of fresh water. They observed that the diameter increases linearly with vertical distance from the source. Their results seemed to confirm the applicability of self-similar entrainment. In an un-stratified environment, a thermal first accelerates to a maximum speed near the source, and decelerates as mixing is accomplished with loss of buoyancy force. The advancing front of a thermal has traditionally been used for measurements since it is a relatively distinctive point (Johari, 1989). A self-similar thermal in the far-field has a width of about half the distance the front traveled (Johari, 1992) while a thermal starting from rest initially exhibits much less entrainment than a self-similar thermal. Grabowski and Clark (1991, 1993) used two and three-dimensional numerical experiments to simulate thermals in a stratified environment and considered cloud-environment interface instability a primary entrainment mechanism.

Linden (1973) proposed a theoretical model based on the impingement of a vortex ring on a stratified interface to explain entrainment results from stirring grid experiments (Turner, 1973). Baines (1975) performed laboratory experiments for the case of an impinging plume. All three studies report an entrainment law proportional to $Ri^{-3/2}$. No observations of interface dynamics are reported by Linden (1973).

Dahm *et al.* (1989) studied the interface dynamics resulting from the impingement of a vortex pair and a vortex ring on a stratified interface. Saunders (1962) and Richards (1962) independently conducted experiments related to a penetrat-

ing thermal into a stably two-layer stratified environment. The penetration height was measured as a function of time (Saunders, 1962) and as a function of the density difference across the interface (Richards, 1962), but neither studied the relationship between penetration height and Richardson number. In both sets of experiments, the density of the thermal and the density difference across the interface were varied simultaneously.

4.6.2 Thermal experiment set-up

An ideal mechanism for releasing thermals would simulate the atmospheric release process as closely as possible. The experimental apparatus described below allows us to create repeatable thermals without imposing initial circulation. The dimensions of the tank used in these experiments are 30 x 30 cm^2 in cross section and 65 cm in height. A vertical cylinder, 2.5 cm inside diameter and 2.9 cm high, is located at the bottom of the tank, in the center, and covered by a thin, horizontal sliding stainless steel lid. For the purpose of generating a thin stratified interface, the tank is separated into two chambers by another thin, horizontal sliding stainless steel plate (Figure 4.14).

The interface is located 15 diameters downstream of the initial thermal diameter, therefore we assume that far field conditions are reached at the interface location. Bond (2001) studied the near field of buoyancy driven vortex rings. The near field was defined as any distance less than 5 nozzle diameters.

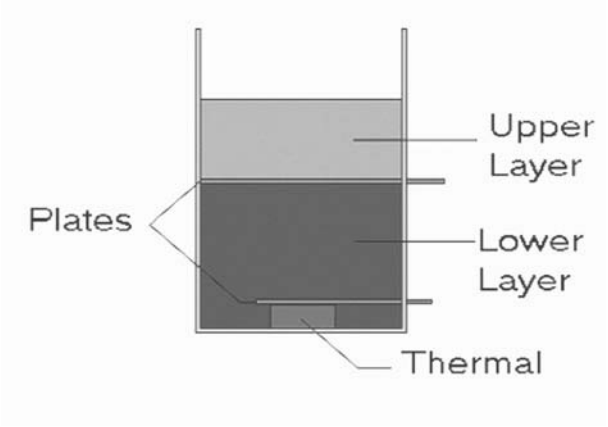

Figure 4.14: Schematic of the experimental set-up for the thermal experiments.

The tank walls are made of chemically resistant lucite to give an unobstructed view of the flow. The top and bottom fluid layers consist of aqueous solutions of different salt concentrations. The density of the lower layer fluid is greater than that of the upper layer fluid, which in turn is greater than the thermal fluid density.

The experimental procedure is the following: the cylinder at the bottom of the tank is filled with freshwater and covered with the sliding lid. Then, the lower section of the tank is filled and the sliding plate is pushed in. Finally fluid is poured into the upper section. The sliding plate and the lid are used to minimize mixing between the different fluids before a run. This allows us to obtain a thin stratified interface, on the order of 4 to 5 millimeters. In addition, no initial circulation is imposed on the thermal before release.

4.6.3 Results

Preliminary experiments of a thermal impinging on a stratified interface have been performed and produced counterintuitive results. Instead of behaving similarly to a vortex ring (Linden, 1973), i.e. rebounding away from the interface, two vortices are created by baroclinic torque from the tilted interface, then these vortices merge with the original thermal vortices to form a vortex pair moving horizontally in the vicinity of the interface (Figures 4.15 and 4.16). No significant vertical transport was observed, as would be expected from the rebound argument.

Zhang and Cotel (2000) measured the entrainment rate of a single thermal impinging on a stratified interface and found it proportional to $Ri^{-3/2}$ as predicted by Cotel and Breidenthal's (1997) persistence theory.

4.7 Conclusions

The new results presented above confirm the wide application of the persistence theory. The entrainment rate across a stratified interface for a thermal; precessing, tilted jet and a sloping gravity current is predicted by the persistence theory.

In the case of the sloping gravity current, shear, through the action of Kelvin-Helmholtz vortices, dominates the entrainment process and therefore a Ri^{-1} power law is observed.

In the case of buoyancy driven flow such as the thermal, the persistence theory applies directly, no stationary eddies are created along the impingement dome, the rebound eddies control the entrainment which is then proportional to $Ri^{-3/2}$.

The forcing mechanism, i.e. buoyancy or momentum has no effect on the entrainment rate; the vortical structure resulting from the impingement is responsible for the type of entrainment that takes place.

The ultimate test for the persistence theory is provided by the precessing and tilted jet experiments. It is found that the entrainment rate is strongly dependent on the strength of the baroclinic vorticity near the interface. The vortical structure of the jet is deeply affected by the tilt angle of the jet. A transition between persistent and non-persistent regimes is observed for a tilt angle between 10° and 15°. A naturally occurring persistent regime can be forced into a non-persistent regime by imposing a sufficiently large precessing speed, which corresponds to a critical value of the persistence parameter for the jet. As a result the entrainment rate of the jet is reduced by at least one order of magnitude.

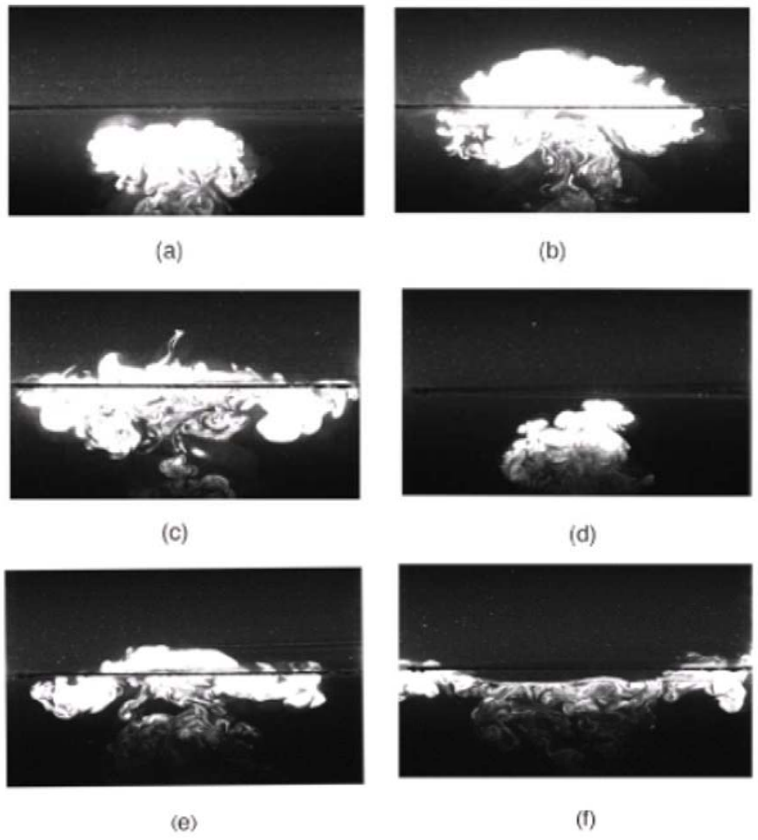

Figure 4.15: Time series of LIF photographs for lower Richardson numbers a) Ri=1.9, t=5s b) Ri=1.9, t=45s c) Ri=1.9, t=80s d) Ri=4.2, t=5s e) Ri=4.2, t=45s f) Ri=4.2, t=80s

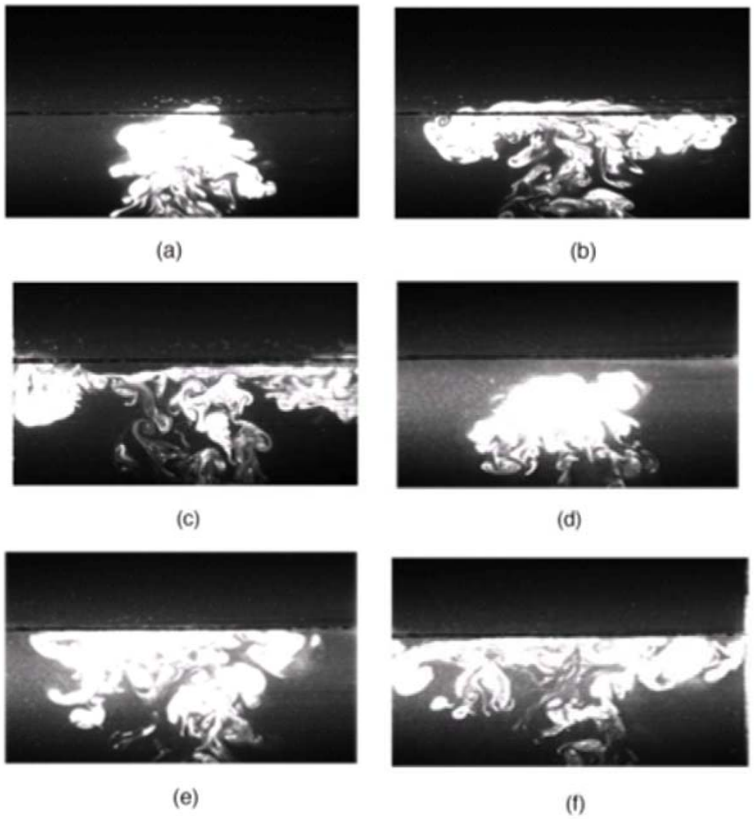

Figure 4.16: Time series of LIF photographs for higher Richardson numbers a)Ri=8.8, t=5s b)Ri=8.8, t=45s c)Ri=8.8, t=80s d) Ri=16, t=5s e)Ri=16, t=45s f)Ri=16, t=80s

4.8 References

Baines W. D.; "Entrainment by a plume or jet at a density interface," *J. Fluid Mech.* **68**, 309-320 (1975).

Beghin P., Hopfinger E. J., Britter R. E.; "Gravitational convection from instantaneous sources on inclined boundaries," *J. Fluid Mech.* **107**, 407-422 (1981).

Benjamin T. B.; "Gravity currents and related phenomena," *J. Fluid Mech.* **31**, 209-248 (1968).

Bond D.; "Near field development of buoyancy driven flows," Master's Thesis, Mechanical Engineering, Worcester Polytechnic Institute (2001).

Britter R .E., Simpson J. E.; "Experiments on the dynamics of a gravity current head," *J. Fluid Mech.* **88**, 223-240 (1978).

Britter R. E., Linden P. F.; "The motion of the front of a gravity current traveling down an incline," *J. Fluid Mech.* **99**, 531-543 (1980).

Brown G. L. and Roshko A.; "On density effects and large structure turbulence," *J. Fluid Mech.* **64**, 775-816 (1974).

Buch E.; "On entrainment and vertical mixing in stably stratified fjord," in *Proc. Int. Symp. Strat. Flows*, Trondheim (1980).

Cotel A. J.; "Entrainment and detrainment of a jet impinging on a stratified interface," Ph.D. Thesis, University of Washington, Seattle (1995).

Cotel A. J. and Breidenthal R. E.; "A model of stratified entrainment using vortex persistence," *Applied Scientific Research*, **57**, 349-366 (1997).

Cotel A. J., Gjestvang J. A., Ramkhelawan N. N. and Breidenthal R. E.; "Laboratory experiments of a jet impinging on a stratified interface," *Experiments in Fluids*, **23**, 155-160 (1997).

Dahm W. J. A. and Dimotakis P. E.; "Measurement of entrainment and mixing in turbulent jets," *AIAA J.* **25**, 1216-1223 (1987).

Dahm W. J. A., Scheil C. M., Tryggvason G.; "Dynamics of vortex interaction with a density interface," *J. Fluid Mech.* **205**, 1-43 (1989).

Fleischmann C. M. and McGrattan K. B.; "Numerical and experimental gravity currents related to backdrafts," *Fire Safety Journal* **33**, 21-34 (1999).

Flynn M. R., Sutherland B. R.; "Intrusive gravity currents and internal gravity wave generation in stratified fluid. *J. Fluid Mech.* **514**, 355-383 (2004).

Gibson C. H., Friehe C. A. and McConnell S. O.; "Structure of sheared turbulent fields," *Phys. Fluids* **20(10)**, S157-S167 (1977).

Grabowski W. W. and Clark T. L.; "Cloud-environment interface instability: Rising thermal calculations in two spatial dimensions," *Journal of the Atmospheric Sciences*, **48**, 527-546 (1991).

Grabowski W. W. and Clark T. L.; "Cloud-environment interface instability. Part II: Extension to three spatial dimensions," *Journal of the Atmospheric Sciences*, **50**, 555-573 (1993).

Hacker J., Linden P. F. , Dalziel S. B.; "Mixing in lock-release gravity currents," *Dynam Atmos Ocean* **24**, 183-195 (1996).

Hallworth M. A., Huppert H. E., Phillips J. C., Sparks S. J.; "Entrainment into two dimensional and axisymmetric turbulent gravity currents," *J Fluid Mech* **308**, 289-311 (1996).

Hopfinger E. J. and Tochon-Danguy J. C.; "A model study of powder-snow avalanches," *Glaciology*, **19**, 343-356 (1977).

Huppert H. E. and Simpson J. E.; "The slumping of gravity currents," *J Fluid Mech* **99**, 785-799 (1980).

Huq P,; "The role of aspect ratio on entrainment rates of instantaneous, axisymmetric finite volume releases of dense fluid," *J Hazard Mater* **49**, 89-101 (1996).

Johari H.; "An experimental investigation of mixing in buoyant flows," Ph. D. Thesis, University of Washington, Seattle (1989).

Johari H.; "Mixing in thermals with and without buoyancy reversal," *Journal of the Atmospheric Sciences* **49(16)**, 1412-1426 (1992).

Jones I. S. and Mulhearn P. J.; "The influence of external turbulence on sheared interfaces," *Geophys. Astrophys. Fluid Dynamics* **24**, 49-62 (1983).

Kneller B. C., Bennett S. J. and McGaffrey W. D.; "Velocity structure, turbulence and fluid stresses in experimental gravity currents," *J. of Geophysical Research-Oceans* **104(C3)**, 5381-5391 (1999).

Kumagai M.; "Turbulent buoyant convection from a source in a confined two-layer region," *J. Fluid Mech.* **147**, 105-131 (1984).

Linden P. F.; "The interaction of a vortex ring with a sharp density interface," *J. Fluid Mech.* **60**, 467-480 (1973).

Lowe R. J., Linden P. F., Rottman J. W.; "A laboratory study of the velocity structure in an intrusive gravity current," *J. Fluid Mech.* **456**, 33-48 (2002).

Maxworthy T., Leilich J., Simpson J. E., Meiburg E. H.; "The propagation of a gravity current into linearly stratified fluid," *J. Fluid Mech.* **453**, 371-394 (2002).

Mitsudera H. and Baines P. G.; "Downslope gravity currents in a continuously stratified environment: a model of the Bass Strait outflow," *11th Australasian Fluid Mechanics Conference*, (1992).

Monaghan J. J.; "Gravity currents and solitary waves," *Physica D* **98**, 523-533 (1996).

Monaghan J. J., Cas R. A. F., Kos A. M., Hallworth M.; "Gravity currents descending a ramp in a stratified tank," *J. Fluid Mech.* **379**, 39-69 (1999).

Morton B. R., Taylor G. I. and Turner J. S.; "Turbulent gravitational convection from maintained and instantaneous sources," *Proc. Roy. Soc. A* **234**, 1-23 (1956).

Mungal M. G. and O'Neil J. M.; "Visual observations of a turbulent-diffusion flame," *Combustion and flame* **78(3-4)**, 377-389 (1989).

Papantoniou D. and List E. J.; "Large scale structure in the far field of buoyant jets," *J. Fluid Mech.* **209**, 151-190 (1989).

Price J. F.; "On the scaling of stress-driven entrainment experiments," *J. Fluid Mech.* **90**, 509-529 (1979).

Richards J. M.; "Experiments on the penetration of an interface by buoyant thermals," *J. Fluid Mech.* **11**, 369-384 (1962).

Roshko A.; "Turbulent shear flow: A new look," *AIAA J.* **14**, 1349-1357 (1976).

Samothrakis P.; "An experimental investigation of the dynamics of a sloping gravity current impinging on a stratified interface," PhD thesis, The University of Michigan, Ann Arbor (2005).

Samothrakis P., Cotel A. J.; "The propagation of a gravity current in a two-layer stratified environment," *J. Geophys. Res.* **111**, C01012 (2006).

Saunders P. M.; "Penetrative convection in stably stratified fluids," *Tellus* **14**, 177-194 (1962).

Schneider G. M., Froud D., Syred N., Nathan G. J. and Luxton R. E.; "Velocity measurements in a precessing flow using a 3-D LDA system," *Experiments in Fluids* **23**, 89-98 (1997).

Schneider H. H.; "Laboratory experiments to simulate the jet-induced erosion of pycnoclines in lakes," *Proc. Int. Start. Flows*, Trondheim (1980).

Scorer R. S.; "Experiments on convection of isolated masses of buoyant fluid," *J. Fluid Mech.* **2**, 583-594 (1957).

Simpson J. E.; "Gravity currents in the laboratory, atmosphere, and ocean," *Ann. Rev. Fluid Mech.* **14**, 213-234 (1982).

Simpson J. E.; "Gravity currents in the environment and the laboratory," 2nd edn. Cambridge University Press (1997).

Sutherland B. R., Kyba P. J., Flynn M. R.; "Intrusive gravity currents in two-layer fluids," *J. Fluid Mech.* **514**, 327-353 (2004).

Turner J. S. and Yang I. K.; "Turbulent mixing at the top of stratocumulus clouds," *J. Fluid Mech.* **17**, 212-224 (1963).

Turner J. S.; "The influence of molecular diffusivity on turbulent entrainment across a density interface," *J. of Fluid Mech.* **33**, 639-656 (1968).

Turner J. S.; "Buoyancy Effects in Fluids," Cambridge University Press (1973).

Whitehead J. A. and Chapman D. C.; "Laboratory observations of a gravity current on a sloping bottom: the generation of shelf waves," *J. Fluid Mech.* **172**, 373-399 (1986).

Winant C. D. and Bratkovich A.; "Structure and mixing with the frontal region of a density current," *Sixth Aust. Hydraul. and Fluid Mech. Conf.*, Adelaide (1977).

Woodward B.; "The motion in and around isolated thermals," *Quarterly Journal of the Meteorological Society* **85**, 144-151 (1959).

Zhang Q. and Cotel A. J.; "Entrainment due to a thermal impinging on a stratified interface with and without buoyancy reversal," *J. Geophys. Research* **105(D12)**, 15,457 - 15,467 (2000).

Zhang X.; "Counter-rotating vortices embedded in a turbulent boundary layer with inclined jets," *AIAA J.*, **37(10)**, 1277-1284 (1999).